Updates to the model of lithium extraction from the Salton Sea Geothermal Field

John O'Sullivan, Theo Renaud, Joris Popineau, and Jeremy Riffault

Department of Engineering Science, University of Auckland, 70 Symonds Street, Grafton, Auckland 1010, New Zealand

jp.osullivan@auckland.ac.nz

Keywords: *Geothermal reservoir simulation, Salton Sea, Lithium, Chloride, Imperial Valley, Waiwera*

ABSTRACT

The Salton Sea Geothermal Field (SSGF) is one of the largest geothermal resources in the world with an estimated resource potential of nearly 3 GW (Kaspereit et al., 2016). It has only been partially exploited due to its high salinity and partial coverage by the Salton Sea. Stakeholders are now focused on better exploiting the field for geothermal energy production and using the lithium-rich geothermal brine as a source of lithium for battery production.

Our numerical model of the SSGF has been used to investigate different options for optimising the extraction of lithium from the system. The model has a chloride-NCG-water equation of state with lithium represented as a passive tracer (Araya and O'Sullivan, 2022, Dobson et al., 2023, O'Sullivan et al., 2023a). It uses a dual porosity approach for the production history and future scenarios to provide an accurate representation of reinjection returns and chemical breakthrough by reinjection fluid that is dilute in lithium. Publicly available data has been used to calibrate both the natural state and production history models.

Most recently future scenarios were run to investigate the influence of the location of reinjection wells on both pressure support and lithium concentrations in the produced geothermal brine. They showed that lithium production can be enhanced without adversely affecting energy production by careful targeting of reinjection. The results of the simulations show the importance of careful monitoring, robust modelling and detailed planning for supporting the extraction of lithium from the SSGF.

To enhance the robustness of the modelling of the SSGF a new round of model development was initiated this year with the support of Lawrence Berkeley National Laboratory and the US Department of Energy's Geothermal Technologies Office. The details of the model development and the forward plan are presented here.

1. INTRODUCTION

The Salton Trough is an active pull-apart basin straddling the Pacific and North American Plates in Southern California. This continental rift zone is characterized by a series of right-stepping dextral faults that link the East Pacific Rise to the San Andreas fault system (Dorsey, 2006). In the extensional gaps between these step-over faults there are a series of smaller spreading centres bounded by northwest-trending strike-slip faults and northeast-trending normal faults (Hulen et al., 2002). The historical development of the Trough is discussed in O'Sullivan et al. (2023a).

Due to crustal thinning and deep magmatic intrusions, the entire Salton Trough experiences an abnormally high heat flux of >100 mW/m^2 (Lachenbruch et al., 1985). Even higher heat flows of >500 mW/m^2 are concentrated in Salton Sea Geothermal Field due to localized Quaternary volcanism and upwelling of hydrothermal fluids (Sass et al., 1984). As a result, significant metamorphic and hydrothermal alteration of the Colorado River sediment occurs at shallower depths in the SSGF (~1.5 km) compared to the rest of the valley (~3 km) (Han et al., 2016).

The brine of the Salton Trough is distinguished by a bimodal distribution of salinity. Cooler less saline brine (<10 wt.% TDS) overlays hot hypersaline brine (>20 wt.% TDS). The hypersaline brines tend to be Na-Ca-K chloride solutions with high concentrations of dissolved metals (Fe, Mn, Zn, Li, Sr) while the less saline brines are typically NaCl solutions with very little dissolved metals (McKibben et al., 1987). These lower salinity brines have chemical compositions very similar to water from the New River and the Salton Sea. While the hypersaline brines have a narrower range of isotopic compositions. Williams and McKibben (1989) state that this indicates active convection and a relatively long residence time.

2. CONCEPTUAL MODEL

This study presents an update of the results from our numerical model used to investigate the thermodynamics of the SSGF and forecast the recoverable lithium potential (Araya and O'Sullivan, 2022, Dobson et al., 2023, O'Sullivan et al., 2023a).

Modelling concepts and workflows described by O'Sullivan et al. (2000), O'Sullivan et al. (2016), Popineau et al. (2018), and O'Sullivan et al. (2023b) as well as Leapfrog Geothermal software, were used to create a digital conceptual model combining geological, alteration, and structural models.

Based on previous work by Wagoner (1980), Dorsey (2006), Dorsey et al. (2011), Kirby et al. (2007), and Hulen et al. (2003), the following seven geologic units were modelled chronologically from oldest to youngest: Crystalline Basement, Imperial Group, Palm Springs Formation, Lower Borrego, Upper Borrego, Brawley Formation, and Alluvium. Regional stratigraphic cross-sections from these studies were used to establish the thickness of each formation. The Borrego Formation was split to capture the dramatic metamorphic and seismic velocity changes that occur at ~1.5 km depths beneath the centre of the SSGF. The crystalline basement surface contact was traced using a regional geological map (California Department of Conservation, 2015).

The Salton Sea sub-basin is dominated by a complex network of blind right-stepping dextral faults and R' Riedel shear faults. The modelled dextral faults include the left

ISSN 2703-4275

strand of the Brawley Fault Zone (Fault I), the right strand of the BSZ (Fault B), Red Hill (Fault R), Calipatria (Fault P), Wister (Fault W), Southern San Andreas (Fault A) and Fault C which was inferred from the alignment of old CO_2 fumaroles and wells (e.g., Svensen et al., 2007; Mazzini et al., 2011; Rao, 2016). These faults were all modelled as having near-vertical dips. They were digitized from maps provided by Kaspereit et al. (2016), Marshall et al. (2022), and Lynch and Hudnut (2008) (Figure 1).

The previously mentioned fault maps in addition to one from McGuire et al. (2015) were used to digitize the R' Riedel shear faults. These faults include the Elmore Ranch (Fault E), Main Central Fault Zone (Fault M), Kalin (Fault K), Hudson (Fault H), Southern boundary (Fault U), Fault T, Butte 1 (Fault V), Butte 2 (Fault X), Butte 3 (Fault Y), Butte 4 (Fault Z).

Four 2D land and offshore resistivity profiles by Nichols (2009) were used to digitally construct the clay cap in the conceptual model. The clay cap was defined as the extremely conductive zone (0.2 to 0.4 Ohm-m). Some uncertainty in the location of the clay cap exists as the combination of high temperature, high salinity, and high porosity can also produce very low resistivity values (Nichols, 2009). Thus, some of the low resistivity anomalies may not actually be part of the clay cap. The landward lateral extent of the clay cap was further refined by resistivity and density maps from Younker et al. (1981).

The conceptual model including stratigraphy, the clay cap and faults is shown in Figure 2.

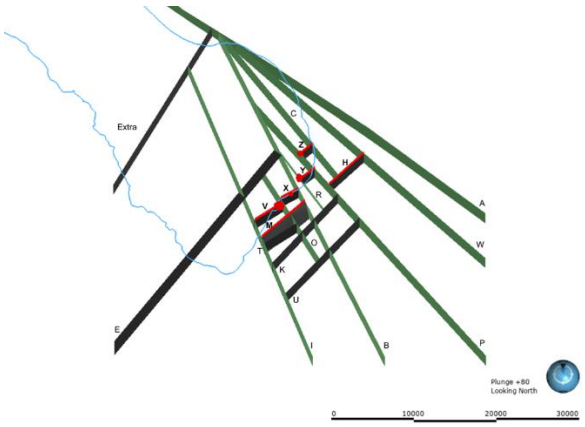

Figure 1: Structural network in the Salton Sea area with local and regional normal faults (Araya and O'Sullivan 2022).

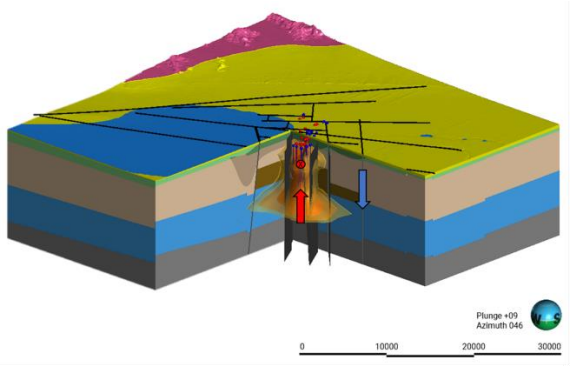

Figure 2: Conceptual model of the Salton Sea Geothermal Field. Salton Sea (blue). Geological units: Granitic Basement (pink), Imperial Formation (grey), Palm Springs (blue), Upper Borrego (tan), Lower Borrego (brown), Brawley (Green), Alluvium (yellow). Select faults shown as black surfaces. Fault traces (black). Shaded zone denotes clay cap. Active production wells (red). Active injection wells (blue). Red arrows show upflow and blue arrows show cold down flow.

3. NUMERICAL MODEL SETTINGS

3.1 Numerical grid and boundary conditions

The 3D conceptual model was discretized into a block model for applying mass and energy balance calculations using the Waiwera geothermal simulator (Croucher et al., 2020). The model was run in the Cloud using 96 core high-performance compute nodes with Amazon Web Services (AWS) or on NeSI.

A grid extending 24 km x 24 km x 3.5 km and oriented along the NE trending axis of the Main Central Fault Zone was created in Leapfrog Geothermal. The grid has a 400 m x 400 m lateral refinement within the SSGF boundary and an 800 m x 800m refinement on the periphery. The grid was designed with a vertical refinement of 25 m near the surface, 50 m at the water table, 100 m in the upper reservoir, 200 m in the lower reservoir, and 500 m at the greatest depths. The final numerical grid consists of 37,688 blocks.

The 'wsce' equation of state in Waiwera was used to include water, salt, carbon dioxide and energy in the thermodynamic calculations and lithium was included in the model as a passive tracer.

The top of the model was assigned two-phase atmospheric conditions of 1 bar and a mean temperature of 23°C on land and a wet atmosphere for the Salton Sea with a temperature of 23°C and a pressure determined by the depth of the sea. The chloride concentration of the Salton Sea was set to a mass fraction of 50,000 ppm. The side boundaries of the grid are located past all bounding faults allowing no-flow lateral boundary conditions to be applied. At the base of the model a background heat flux of 150 mW/ m² was applied with an additional 136 MW applied as heat and mass inputs under the SSGF representing the deep geothermal upflow. Figure 3 shows the applied variable higher heat flux in the central part of 400 mW/m², surrounded by a zone of 250 mW/m². Chloride was included in the deep upflow at a mass fraction equivalent to 152,000 ppm and lithium at a concentration of

ISSN 2703-4275

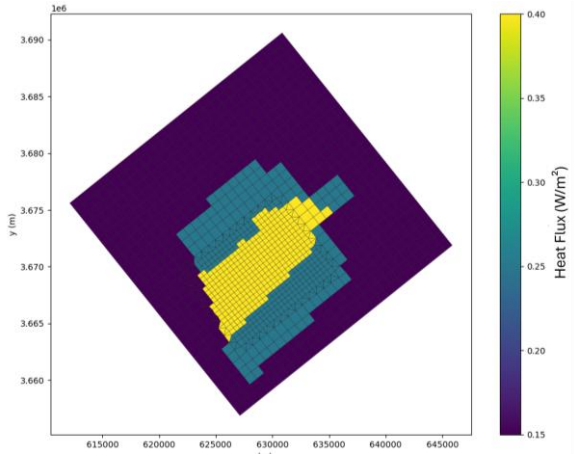

Figure 3: Heat fluxes area at the bottom of the SSGF numerical model.

220 ppm, a ratio of 682:1. The CO_2 mass fraction coming for deeper sources are set at 0.2% in the deep upflows of water.

The model used 561 rock-types covering the combinations of lithology, fault zone, fault zone intersections, and alteration that are included in the conceptual model. Many rock-type classifications share common permeability and porosity values, but the large number of combinations allows a high level of heterogeneity in the permeability and porosity distributions as required. Other secondary rock properties (density, heat conductivity, and rock grain-specific) were held constant across all rock-type classifications.

During production and future scenario runs, a dual-porosity model was used to capture reinjection returns more accurately. The dual-porosity parameters are given in Table 1 below.

Table 1: Dual porosity parameters used in the production history model and future scenarios.

Parameter	Value
Number of matrix blocks	2 (20% and 77.5%)
Volume fraction of fracture blocks	2.5%
Fracture spacing	25 m
Fracture planes	3
Permeability of matrix	1.0E-16 m^2
Permeability of fractures	variable
Porosity of fractures	80 %

3.2 Historical data

Static temperature and brine chemistry data from exploration wells drilled prior to the start of 1980s commercial production were compiled from studies by Helgeson (1968), Palmer (1975), and Sass et al. (1988). Helgeson (1968) obtained temperature measurements over a three-year period for the following eight wells: IID 1, IID 2, IID 3, River Ranch 1, Sinclair 3, Sportsman 1, Elmore 1, and State 1. Palmer (1975) compiled temperature and brine chemistry data from MagMaMax 1, MagMaMax 2, MagMaMax 3, and Woolsey 1. Lastly, Sass et al. (1988) analyzed temperature data from the State 2-14 well to construct an equilibrated static temperature profile.

Static temperature surveys for Lander 2, Elmore IW-4, River Ranch 17, Fee 5, and Vonderahe 1 were collected from CalGEM's GeoSteam data repository. Most of these temperature profiles exhibit a change from a conductive to a convective gradient between depths of 600 to 900 m. This break corresponds well with the average depth of the impermeable clay cap (Sass et al., 1988).

CalGEM's GeoSteam database was used to obtain monthly production and injection data for all the active production and injection wells in the SSGF. These monthly production/injection reports document the average monthly TDS, discharge temperature, wellhead pressure, steam mass rate, and brine mass rate. The GeoSteam database was also used to get well schematics, directional surveys, mud logs, static PTS logs, and well history reports for all the active production and injection wells. Well schematics provided wellhead coordinates, KB, ground level, and total measured depth. Total and/or partial circulation zones that were noted in the mud logs were used to infer feed zones. This was the best approach given the lack of proprietary well-testing and feed zone data.

3.3 Future Scenario set up

Three scenarios were defined in O'Sullivan et al. 2024 to investigate the lithium extraction process, with different lithium production rates modelled over the next 20 years.

The scenario assumed that all reinjection rates are constant for all reinjection wells. The production wells are set on deliverability. The reinjected chloride concentrations also remain constant for the full period. However, from 01/01/2024 the lithium concentration for all reinjection wells was reduced by 95%, which is representative of a future scenario where technology allows for 95% of the lithium in the brine to be extracted before reinjection. Figure 4 shows the location of the makeup injection wells outside the existing production and injection wells. The scenarios are set up using the current production and reinjection wells at the end of the production history and future peripherical reinjection wells. Table 2 shows the parameters for the simulations of the future scenarios.

Table 2: Scenario parameters

Scenario	lithium reinjected (%)	Make up wells	Mass reinjected Field Total ≈ 12500 t/h
S1	5	0	Following last reinjection data in 2023
S2	5	36	360 t/h in each future injection well
S3	5	36	600 t/h in the deep future injection wells 120 t/h in the intermediate future injection wells.

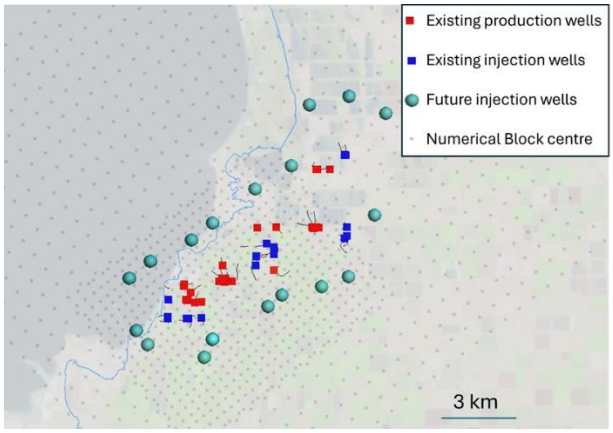

Figure 4: Locations of the make-up injection wells for Scenario 2 and Scenario 3 with the existing production and injection wells. The shaded black dots are the numerical grid block centre. The Salton Sea shoreline in 1986 is shown in light blue.

Scenario S1 uses the current sets of production and reinjection wells without any make-up wells. For all three scenarios the existing production wells were put on to deliverability and no new production wells were added.

Scenario S2 and S3 investigate reinjection plans by targeting the periphery of the production reservoir with new reinjection wells. The location of each future injection well corresponds to two wells per well pad. The total amount of reinjected fluid and reinjection enthalpy are kept constant for all three scenarios. The objective is to target the intermediate depths of the reservoir (-1000 masl to -1400 masl) with one future injection well and the deeper part of the reservoir (-1400 masl to -2400 masl) with the second injection well.

For Scenarios 2 and 3, 18 new reinjection wells target intermediate depths, and 18 new reinjection wells target the deep reservoir. In Scenario 2 the total reinjection was split evenly between the wells resulting in 360 t/h being reinjected into each well. In Scenario 3 the deep reservoir was targeted more heavily with 600 t/h reinjected into the deep wells and 120 t/h into the intermediate wells. The objective of Scenario 3 was to slow down the thermal breakthrough occurring in the more permeably intermediate layers of the production reservoir. All three scenarios are run for 20 years with the lithium extraction process beginning at the start of the second year. It was assumed that there will still be 5% of the lithium remaining in the reinjected mixture of water and dissolved salts.

5. RESULT AND DISCUSSION

5.1 Natural State model

The natural state model was calibrated following standard practice by adjusting the permeability distribution and deep geothermal inputs at the bottom boundary of the model. A good calibration of the model (Araya and O'Sullivan, 2022) had already been achieved, matching measured downhole temperatures. However, the addition of chloride significantly affected the thermodynamics of the system requiring substantial re-calibration of the enhanced model.

Figure 5 shows a selection of wells with downhole temperature data and the modelled temperatures. Despite not having high temperatures at great depth, the match is good. This is a challenging task as some measured temperatures are close to 360°C which is the limit of application for the current version of the Waiwera simulator.

Results from the calibration process demonstrate that the infield R'Riedel shear faults and dextral strike slip faults are the main drivers of vertical upflow (see Figure 5). Hot upflow is concentrated along Faults M, V, X, Y, O, and I. The reservoir is bounded in the k1 horizontal direction by Faults E, T, K, and U. These R' shear faults limit outflow to the south and to the northwest. The reservoir is bounded in the k2 horizontal direction mainly by Faults I, O, B, P, W, and A. The clay cap acts as an upper boundary to vertical fluid flow. The clay cap is thickest in the NW of the Sea where it acts as a lateral boundary to northeast outflow. Lastly, the periphery dextral faults (U, K, W, and A) act as large conduits for cold shallow infiltration.

As well as calibrating the temperature distribution, the model permeability distribution was adjusted to produce a chloride distribution consistent with the measured data. In particular, the aim was to reproduce the deep hypersaline reservoir overlaid with an intermediate mixing zone and a low-chloride shallow zone. Overall, it captures the deep hypersaline reservoir and the intermediate mixing zone. However, in the model the deep hypersaline fluid penetrates the shallow zone over a much larger area than has been observed. More model calibration is required, reducing permeabilities in the vertical pathways between the deep reservoir and the shallow system to reduce the upflow of hypersaline fluid. Lithium is included in the natural state model as a passive tracer with its concentration coupled closely to the chloride concentration.

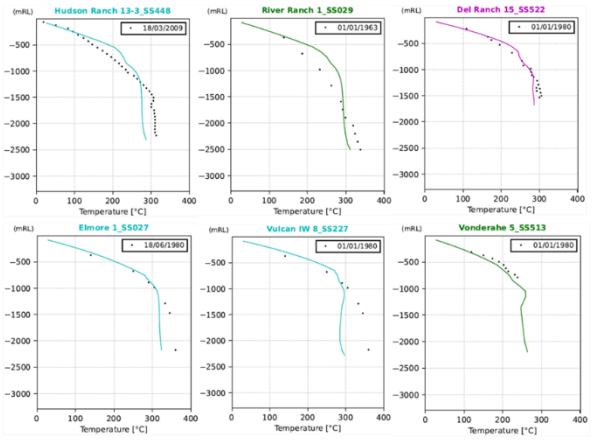

Figure 5: Natural state downhole temperatures for selected wells. Model results are shown as coloured lines and measured data as points (O'Sullivan et al. 2024).

5.2 Production model

The production model was set up using our standardized framework for including production and reinjection wells (O'Sullivan et al., 2023). This approach adds wells as time dependent source and sink terms in the model blocks corresponding to the feed zones of the production and reinjection wells. The model was then run for the corresponding production history time period and calibrated to match measured transient data for production enthalpies and chloride mass fractions. For the reinjection wells the enthalpy of the reinjected fluid and its chloride concentration are model inputs taken from measured data. The lithium concentration for the reinjection fluid was assumed to remain constant at a ratio of 682:1 to the measured chloride, as no appreciable amount of lithium has historically been extracted from the brine.

Figure 6 shows the production model results and data collected for the lithium and salt mass fraction in three wells in the area. The calibration achieved was satisfactory for carrying on with investigations of future scenarios.

Without information on changes in the feedzone elevation over time which may alter the chemical composition of produced fluids, these wells highlight a breakthrough of the higher chloride concentration from the lower enthalpy reinjection fluids. Lithium concentration increases due to a higher lithium concentration in the reinjected fluid than in the reservoir.

The rate of thermal and chemical breakthrough as a result of reinjection is dependent on the permeability and porosity distributions, the location of the production and the reinjection wells and their feedzones, and the rates of production and reinjection.

The increased chloride concentrations are distributed heterogeneously across the field as a result of faults, formations and differences in production and reinjection elevations. Figure 7 shows the model results matching the CO_2 mass fraction in the produced fluids of the wells Elmore 12, M 10 and Vonderahe 3 with good agreement. In other areas, using a uniform CO_2 ratio from the deep water upflows in the model seems to underestimate the amount of CO_2 in the well River Ranch 11 and Del Ranch 12 compared to the historical measurements.

The current model does a good job of matching the overall behaviour of the SSGF and the dual-porosity approach allows a good representation for the reinjection returns. However, more calibration, more detailed calibration data and a more refined model grid would allow for more accurate representation of the historic changes in the chloride, lithium concentrations and CO_2 content.

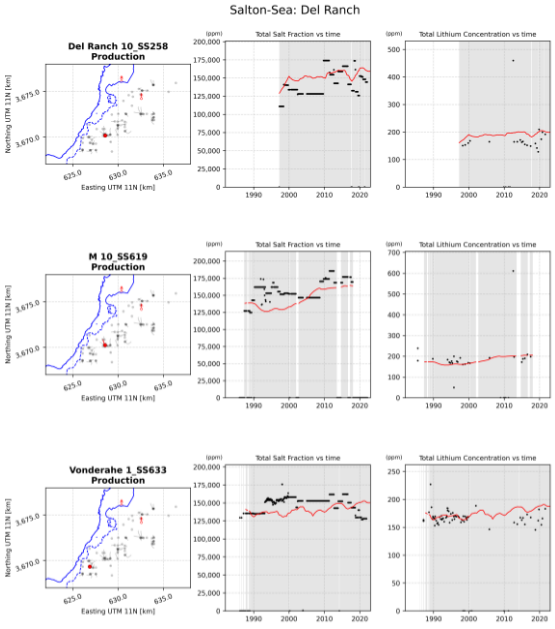

Figure 6: Production model results for well Del Ranch 10 M 10, Vonderahe 1 for the Chloride mass Fraction and Lithium

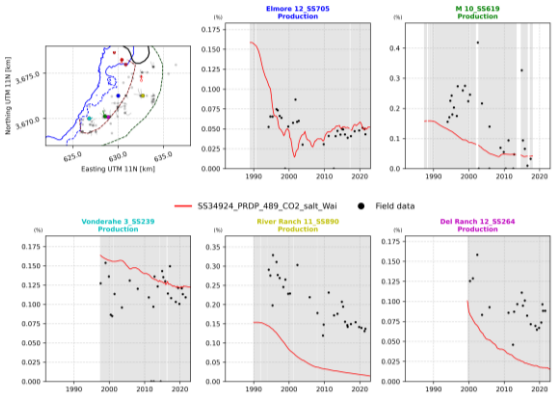

Figure 7: Model results of the CO_2 mass fraction in the produced fluids compared to the data collected in the selected wells of the Salton Sea Geothermal Field.

5.3 Future Scenarios

Figure 8 shows the horizontal distribution of the lithium concentration at the depth of -1250 masl in 2030 for the three scenarios modelled. The location of the reinjection wells and the depth of the reinjection targets shows the impacts on the lithium distribution might be out of the reach of existing production wells. This approach also provides information about future locations of the production wells to target zones of high lithium concentration.

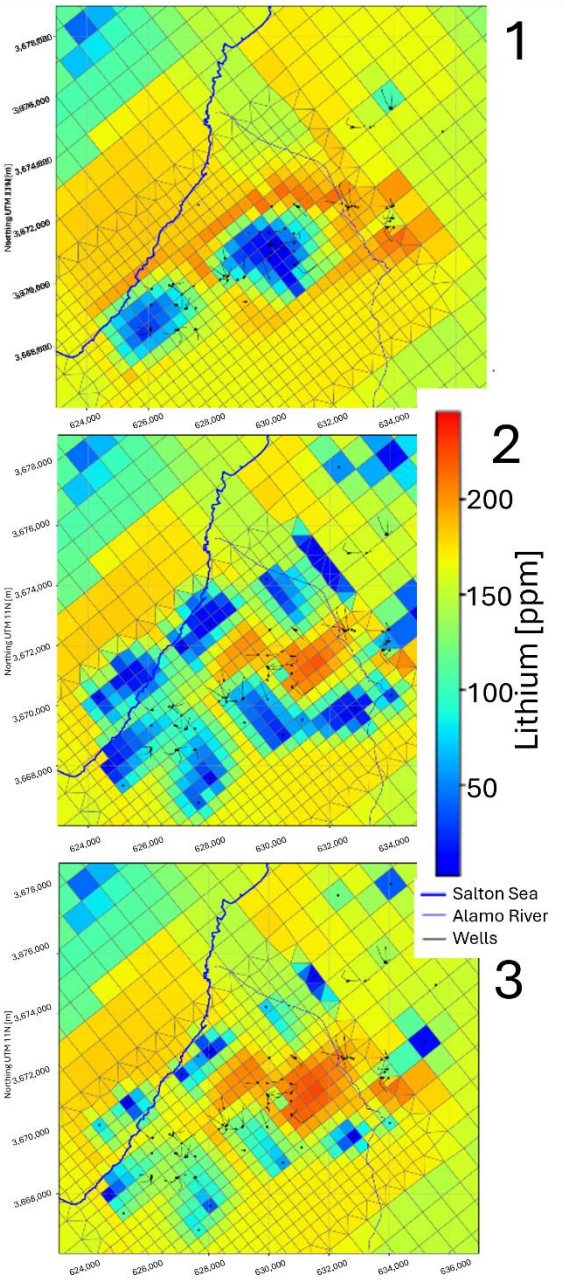

Figure 8: Comparison of forecast lithium distribution in the intermediate reservoir at -1250 masl in 2030 for (1) Scenario 1, (2) Scenario 2 and (3) Scenario 3 (O'Sullivan et al. 2024).

The total amounts of lithium extracted over the 19 years of production are given in Table 3 for all three scenarios. It shows that Scenario 3 is forecast to provide nearly 30% more lithium compared with Scenario 1 by optimizing the reinjection targets.

The total amount of lithium forecast to be produced in Scenarios 1, 2 & 3 is shown in Figure 9. The decline in forecast lithium production is a result of chemical breakthrough from the reinjected fluid with a low lithium concentration. Some areas in the reservoir are predicted to have already experienced dilution of the lithium concentration (O'Sullivan et al. 2024). This is a result of reinjection of condensate with a low concentration of lithium in particular wells.

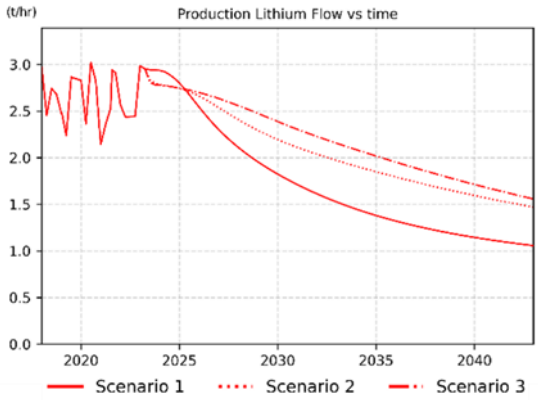

Figure 9: Total production lithium flow for Scenarios 1,2,3 (O'Sullivan et al. 2024).

Table 3: Forecasts of total lithium extracted for each scenario over 19 years of production (O'Sullivan et al. 2024).

Scenario	Forecast Lithium Extracted (kg)
1	278,000,000
2	338,000,000
3	360,000,000

As discussed above, none of the scenarios considered additional production wells. Optimising both production and reinjection targets will certainly enable higher production rates of both lithium and energy to be achieved.

6. MODEL DEVELOPMENT AND FORWARD PLAN

To enhance the robustness of the modelling of the SSGF a new round of model development was initiated this year with the support of Lawrence Berkeley National Laboratory and the US Department of Energy's Geothermal Technologies Office. The project has four main work streams to improve and extend the previous model.

6.1 Increased model resolution in the production zone

The previous model is relatively coarse at 400 m x 400 m in the production zone. We have reduced this to 200 m x 200 m and extended the zone covered by the 400 m x 400 m resolution (see Figure 10 and Table 4). Model resolution in the production zone affects the accuracy of model forecasts, particularly for reinjection returns which is a key driver for forecasting lithium production rates over time. A higher resolution model will also allow us to better represent structural controls on the SSGF thus improving the quality of forecasts.

a)

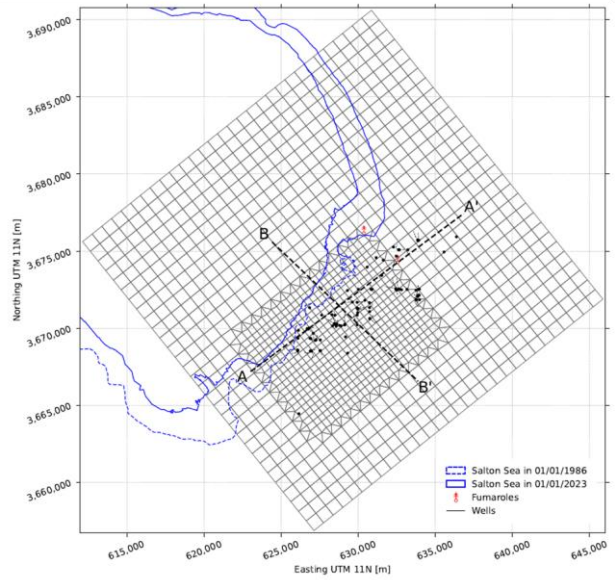

b)

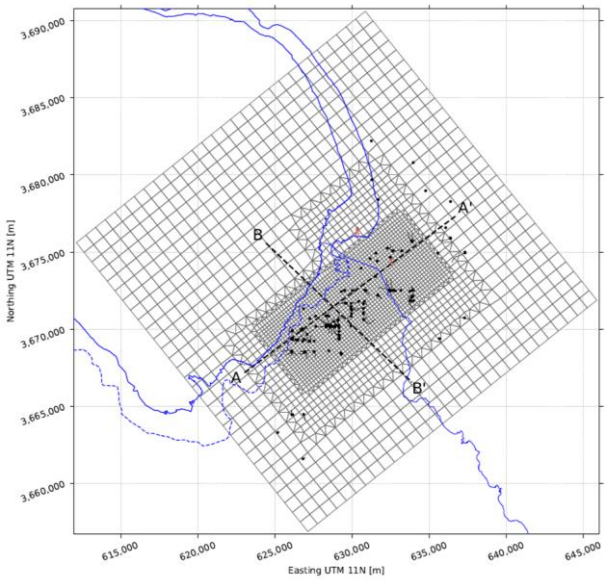

Figure 10: Comparison of a) previous model grid and b) new model grid.

6.2 Improved model calibration

Improved model calibration improves the quality of the model forecasts and will give more confidence to stakeholders in our modelling results. We have also carried a more in-depth analysis of the publicly available production data and added 14 production and 15 production wells to the dataset (see Table 4). Also, the production data have been extended from December 2023 to June 2024 and available lithium and CO_2 mass fraction data have been added.

Table 4: Comparison of model grids and calibration data sets.

	Previous Version	New Version
Grid size	34924	92186
Production Wells	28	62
Reinjection wells	42	57
Final Dates	December 2023	June 2024

6.3 More realistic lithium production scenarios

The future scenario run in the first stage of the project was a simple, somewhat naïve approach to lithium extraction designed to understand the overall response of the SSGF. All the reinjection was assumed to have 95% of the lithium removed after 01/01/2024 and all production and reinjection rates were assumed to remain at current rates. Several more informative scenarios need to be tested. These would be identified in consultation with the wider project team and would include, but would not be limited to:

1. A staged approach to lithium removal
2. Investigating the effects different rates of geothermal energy production
3. Targeted reinjection to extract lithium more efficiently

6.4 Uncertainty quantification of model forecasts

A key issue with geothermal reservoir model forecasts is uncertainty arising from uncertain model parameters and uncertainty in the measured data used for model calibration. This is issue is particularly problematic when we do not have access to the full set of measured data such as is the case for the SSGF. Even in projects where the full measured data set is available, there are usually many uncertainties due to data gaps, measurement errors and operational constraints in monitoring. The best approach for addressing this problem is carrying out a formal uncertainty quantification of the geothermal model forecasts. Our group has pioneered uncertainty quantification for geothermal models and have successfully applied our methodology to several commercial projects. We have also published several articles on our approach (de Beer et al., 2023, Dekkers et al. 2022). Producing forecasts of lithium production from the SSGF that include uncertainty quantification would not only consider limitations in the measured data but would also give much better support for long term decision making.

6.5 Techno-economic analysis

Like energy, the economic viability of harvesting lithium from a reservoir is better understood with the inclusion of reservoir physics, wellbore physics, and realistic extraction and reinjection scenarios. We will develop and apply a techno-economic analysis (TEA) framework to evaluating the economics of energy and lithium recovery scenarios in the Salton Sea region.

This will be accomplished by coupling temporal forecasts of the lithium and energy resource from our reservoir models

with cost and operation data for well operation gathered from literature, and with a TEA model of a hybrid geothermal facilities with lithium extraction capabilities, developed by LBNL for the California Energy Commission. The model is based on process simulations run in ASPEN software for brine data provided by companies in the Salton Sea. We will modify the model to account for variations in brine composition, temperature, and flow rates. A robust sensitivity analysis will be conducted to help bound uncertainties related to key cost drivers such as the performance of technologies over time.

6. CONCLUSION

We have developed an integrated detailed model of the SSGF to investigate the distribution of Lithium in the area. The collection of a large amount of reservoir engineering data from the old and current production and reinjection wells, along with chemical information on the fluids was conducted to obtain as much information as possible to quantify the sustainably extractable energy and lithium in the area.

The modelling study investigated the use of targeted reinjection strategies to extract lithium efficiently from the SSGF. The results show that the production rates of lithium can be increased by nearly 30% by moving reinjection to the periphery of the production zone and preferentially targeting deep reinjection. Improved lithium extraction rates were achieved without severe impacts on energy production rates.

The results from our previous modelling studies provided valuable insights into the lithium production potential from the SSGF and demonstrated that our model can produce high quality modelling forecasts consistent with conceptual understanding of the system. This year we have initiated a new phase of model development to improve the reservoir model allowing it to provide more robust forecasts and carry out more detailed studies. A Techno-Economic Analysis will also be carried out combining the reservoir modelling outputs with important economic factors to support strategic decision-making around the SSGF resource.

ACKNOWLEDGEMENTS

We would like to thank Bentley Systems for providing the user license for Leapfrog Energy and their ongoing collaboration and support, and NeSI for supporting this research.

The authors would like to thank the Lawrence Berkeley National Laboratory and the Department of Energy's Geothermal Technologies Office for supporting this project.

REFERENCES

Araya, N. and O'Sullivan, J. "A 3D Conceptual and Natural-State Model of the Salton Sea Geothermal Field." GRC Transactions, 46, (2022). 2123-2155.

CalGEM. "GeoSteam: Geothermal Well Records, Production and Injection Data [Data Files]." (2022). https://geosteam.conservation.ca.gov/

California Department of Conservation. "Geological Map of California [Data File]." (2015). https://maps.conservation.ca.gov/cgs/#datalist

California Department of Conservation. "Geothermal Production and Injection Data [Salton Sea]." (2022). https://www.conservation.ca.gov/calgem/geothermal/manual

Croucher, A., O'Sullivan, M., O'Sullivan, J., Yeh, A., and Burnell, J. "Waiwera: A parallel open-source geothermal flow simulator." Computers and Geosciences, 141, (2020).

de Beer, A., Gravatt, M., Renaud, T., Nicholson, R., Maclaren, O. J., Dekkers, K., O'Sullivan, M., O'Sullivan, J., "Geologically Consistent Prior Parameter Distributions for Uncertainty Quantification of Geothermal Reservoirs." 48th Stanford Workshop on Geothermal Reservoir Engineering, California, (2023).

Dekkers, K., Gravatt, M., Maclaren, O. J., Nicholson, R., Nugraha, R., O'Sullivan, M., O'Sullivan, J., "Resource Assessment: Estimating the Potential of a Geothermal Reservoir." 47th Stanford Workshop on Geothermal Reservoir Engineering, California, (2022).

Dobson, P., Araya, N., Brounce, M., Busse, M., Camarillo, M. K., English, L., ... & White, M. (2023). Characterizing the Geothermal Lithium Resource at the Salton Sea. Lawrence Berkeley National Laboratory (LBNL), Berkeley, USA.

Dorsey, R. "Stratigraphy, Tectonics, and Basin Evolution in the Anza-Borrego Desert Region." In G. T. Jefferson and L. Lindsay, Fossil Treasures of the Anza-Borrego Desert, Sunbelt Publication, (2006) 89-104.

Han, L., Hole, J.A., Stock, J.M., Fuis, G.S., Kell, A., Driscoll, N.W., Kent, G.M., Harding, A.J., Rymer, M.J., González-Fernández, A., and Lázaro-Mancilla, O. "Continental rupture and the creation of new crust in the Salton Trough rift, Southern California and northern Mexico: Results from the Salton Seismic Imaging Project." Journal of Geophysical Research: Solid Earth, 121, (2016), 7469-7489.

Hulen, J., Kaspereit, D., Norton, D.L., Osborn, W., Pulka, F.S. "Refined Conceptual Modeling and a New Resource Estimate for the Salton Sea Geothermal Field, Imperial Valley, California." Geothermal Resources Council Transactions, 26, (2002), 29-36.

Hulen, J., Norton, D., Kaspereit, D., Murray, L., Van de Putte, T., and Wright, M. "Geology and a Working Conceptual Model of the Obsidian Butte (Unit 6) Sector of the Salton Sea Geothermal Field, California." GRC Transactions, 27, (2003), 227-240.

Kaspereit, D., Mann, M., Sanyal S., Rickard, B., Osborn, W., and Hulen, J. "Updated Conceptual Model and Reserve Estimate for the Salton Sea Geothermal Field, Imperial Valley, California." GRC Transactions, 40, (2016), 57-66.

Kirby, S.M., Janecke, S.U., Dorsey, R.J., Housen, B.A, Langenheim, V.E., McDougall, K.A., and Steely, A.N. "Pleistocene Brawley and Ocotillo Formations: Evidence for Initial Strike-Slip Deformation Along the San Felipe and San Jacinto Fault Zones, Southern California." Journal of Geology, 115, (2007).

Lachenbruch, A.H., Sass, J.H., and Galanis, S.P. Jr. "Heat flow in southernmost California and the origin of the Salton Trough." Journal of Geophysical Research, 90 (B8), (1985), 6709-6736.

Lynch, D.K., and Hudnut, K.W. "The Wister Mud Pot Lineament: Southeastward Extension or Abandoned Strand of the San Andreas Fault?" Bulletin of Seismological Society of America, 98, (2008), 1720-1729.

Marshall, S., Plesch, A., Shaw, J., and Nicholson, C. "SCEC Community Fault Model v. 5.3.2." (2022). https://www.scec.org/research/cfm-viewer/

Mazzini, A., Svensen, H., Etiope, G., Onderrdonk, N., and Banks, D. "Fluid origin, gas fluxes and plumbing system in the sediment-hosted Salton Sea geothermal system (California, USA)." Journal of Volcanology and Geothermal Research, 205, (2011), 67-83.

Meidav, T., West, R., Katzenstein, A., and Rostein, Y. "An Electrical Resistivity Survey of the Salton Sea Geothermal Field, Imperial Valley California." Lawrence Livermore Laboratory, UCRL-13690, (1976).

McKibben, M.A., Elders W.A., and Raju A.S.K. "Crisis at the Salton Sea: Lithium and Otherm Geothermal Mineral and Energy Resources Beneath the Salton Sea." Crisis at the Salton Sea: The Vital Role of Science, University of California Riverside Salton Sea Task Force, (2021), 74-85.

McKibben, M. A., and Hardie, L. A. "Ore-forming brines in active continental rifts." Geochemistry of Hydrothermal Ore Deposits, 3rd Edition, (1997), 875–933.

McKibben, M.A., Williams, A.E., Elders, W.A., and Eldridge, C.S. "Saline brines and Metallogenesis in a Modern Sediment-filled Rift: the Salton Sea Geothermal system, California, U.S.A." Applied Geochemistry, 2, (1987), 563-578.

McGuire, J.J., Lohman, R.B., Catchings, R.D., Rymer, M.J., and Goldman, M.R. "Relationships Among Seismic Velocity, Metamorphism, and Seismic and Aseismic Fault Slip in the Salton Sea Geothermal Field region." Journal of Geophysical Research, 120, (2015), 2600-2615.

Nichols, E. "Geothermal Exploration Under the Salton Sea Using Marine Magnetotellurics." California Energy Commission, PIER Renewable Energy Technologies Program, CEC-500-2009-005, (2009).

Norton and Hulen. "Magma-Hydrothermal Activity in the Salton Sea Geothermal Field Imperial County, California." GRC Transactions, 30, (2006). 991-998.

Omagbon, J., Doherty, J., Yeh, A., Colina, R., O'Sullivan, J., McDowell, J., . . . O'Sullivan, M. "Case studies of predictive uncertainty quantification for geothermal models." Geothermics. 97, (2021), 102263.

Rao, A.P. "The hydraulic connectivity, perennial warming and relationship to seismicity of the Davis-Schrimpf seep field, Salton Trough, California from new and recent temperature time-series." M.S. thesis, California State University, Long Beach, (2016), 107 p.

Svensen, H., Karlsen, D.A., Sturz, A., Backer-Owe, K., Banks, D.A., and Planke, S. "Processes Controlling Water and Hydrocarbon Composition in Seeps from the Salton Sea Geothermal System, California, USA." Geology, 35, (2007), 85-88.

O'Sullivan, J., Araya, N., Popineau, J., Renaud, T., and Riffault, J. "An EWASG Natural State and Production Forecast Model of the Salton Sea Geothermal Field." GRC Transactions, 47, (2023).

O'Sullivan, M., Pruess, K., and Lippmann, M. "Geothermal Reservoir Simulation: The state-of Practice and Emerging trends." Proceedings World Geothermal Congress, (2000).

O'Sullivan, M., & O'Sullivan, J. "Reservoir Modeling and Simulation for Geothermal Resource Characterization and Evaluation." Geothermal Power Generation, (2016), 165-199.

O'Sullivan, J.P., Araya, N., Popineau, J., Renaud, T., & Jeremy Riffault, J. "An EWASG Natural State and Production Forecast Model of the Salton Sea Geothermal Field", Transactions GRC, 47 (2023a).

O'Sullivan, J., Popineau, J., Gravatt, M., Renaud, T., Riffault, J., Croucher, A., Yeh, A. & O'Sullivan M. "An integrated, mesh-independent geothermal modeling framework." Environmental Modeling and Software, 163, (2023b), 105666.

O'Sullivan, J., Araya, N., Popineau, J., Renaud, T., Riffault, J and O'Sullivan M. Investigating Reinjection Strategies to Optimise Lithium Production from the Salton Sea Geothermal Field. 49th Workshop on Geothermal Reservoir Engineering Stanford University, Stanford, California, February 12-14, (2024)

Palmer, T.D. "Characteristics of Geothermal Wells Located in the Salton Sea Geothermal Field, Imperial County, California." Lawrence Livermore Laboratory, UCRL-51976, (1975).

Popineau, J., O'Sullivan, J., O'Sullivan, M., Archer, R., and Williams, B. "An integrated Leapfrog /TOUGH2 Workflow for a Geothermal Production Modeling." 7th African Rift Geothermal Conference, (2018).

ISSN 2703-4275

Sass, J.H., Galanis, S.P., Jr., Lachenbruch, A.H., Marshall, B.V., and Munroe, R.J. “Temperature, Thermal Conductivity, Heat Flow, and Radiogenic Heat Production from Unconsolidated Sediments of the Imperial Valley, California.” USGS Open File Report, 84-490, (1984).

Sass, J.H., Priest, S.S., Duda, L.E., Carson, C.C., Hendricks, J.D., and Robison, L.C. “Thermal Regime of the State 2-14 well, Salton Sea Scientific Drilling Project.” Journal of Geophysical Research, 93 (B11), (1988), 12,995-13,004.

Williams, A.E., and McKibben, M.A. “A Brine Interface in the Salton Sea Geothermal System California: Fluid Geochemical and Isotopic Characteristics.” Geochimica et Cosochimica Acta, 53, (1989), 1905-1920.

Younker, L.W., Kasameyer, P.W., and Tewhey, J.D. “Geological, Geophysical, and Thermal Characteristics of the Salton Sea Geothermal Field, California.” Journal of Volcanology and Geothermal Research, 12, (1981), 221-258.

ISSN 2703-4275